Materials Science in Semiconductor Processing 68 (2017) 140–146

Contents lists available at ScienceDirect

Materials Science in Semiconductor Processing

journal homepage: www.elsevier.com/locate/mssp

$SrTi_{1-y}Fe_yO_3$ samples obtained by hydrothermal method: The effect of the amount of Fe on structural and photocatalytic properties

Henrique A.J.L. Mourão[a,*], Osmando F. Lopes[b,c], Waldir Avansi Jr[d], Manoel J.M. Pires[a], Solange Souza[a], Cauê Ribeiro[c], Valmor R. Mastelaro[e]

[a] Universidade Federal dos Vales do Jequitinhonha e Mucuri (UFVJM), Instituto de Ciência e Tecnologia, Diamantina/MG, CEP 39100-000, Brasil
[b] Universidade Federal de São Carlos (UFSCar), Departamento de Química, Rod. Washington Luiz, km 235, CEP 13565-905 São Carlos/SP, Brasil
[c] EMBRAPA Instrumentação, Rua XV de Novembro, 1452, CEP 13560-970, CP 741, São Carlos/SP, Brasil
[d] Universidade Federal de São Carlos (UFSCar), Departamento de Física, Rod. Washington Luiz, km 235, CEP 13565-905 São Carlos/SP, Brasil
[e] Instituto de Física de São Carlos, Universidade de São Paulo, Avenida Trabalhador São-carlense, 400, 13566-590 São Carlos/SP, Brasil

ARTICLE INFO

Keywords:
Strontium titanate
Iron (Fe)
XAS
Mössbauer spectroscopy
Photocatalysis

ABSTRACT

This manuscript describes the synthesis and the photocatalytic efficiency of $SrTiO_3$ (STO) and $SrTi_{1-y}Fe_yO_3$ (STFO, with 2.5, 5, 10, 25 and 40 mol% of Fe) materials evaluated by monitoring the photodegradation of methylene blue (MB) dye under visible and UVC irradiation. Samples synthesized by conventional hydrothermal method were characterized by X-ray diffraction (XRD), scanning electron microscopy (SEM), N_2 adsorption isotherms, UV–Vis diffuse reflectance spectroscopy (DRS), X-ray absorption spectroscopy (XAS) and Mössbauer spectroscopy. The results show that a controlled introduction of Fe into Ti sites caused changes in morphology, local order, band gap, textural properties and photoactivity of the STO compound. By increasing the Fe content, the surface roughness was also increased when compared with the STO sample. Furthermore, the highest amount of Fe caused significant changes in the STO lattice, especially in relation to the local order around Ti atoms. The Mössbauer analysis confirmed that Ti^{4+} atoms were replaced by Fe^{3+}. The sample with the lower amount of Fe (2.5 mol%) presented photoactivity similar to that of pure STO. The samples containing intermediate amounts of Fe (5 and 10 mol%) presented good performances on the methylene blue (MB) dye photodegradation, while others with higher amounts of Fe (25 and 40 mol%) led to a large distortion of the crystalline structure, which disfavored the photocatalytic performance. The enhanced photoactivity of the some STFO samples was related to three combined effects: an improvement of the textural property; a decrease in the rate of electron-hole recombination; and a broadening of the photocatalyst optical absorption band, which is important for the photodegradation under visible irradiation. These positive characteristics were predominant for both 5 mol% and 10 mol% STFO samples. The one with 5 mol% has presented the best performance for MB photodegradation, which was mainly attributed to its best textural properties.

1. Introduction

Materials with perovskite structure generally show notable properties, including a large group of compounds that can be represented by the ABO_3 chemical formula. Among such materials, strontium titanate ($SrTiO_3$ or just STO) has been widely studied for different applications, such as gas sensors and photocatalysts [1–4]. The STO is considered an important n-type semiconductor with band gap of approximately 3.2 eV [1]. In the perovskite STO structure, Sr^{2+} ions occupy site 'A', while Ti^{4+} ions are located in site 'B,' although the STO lattice can accommodate several atoms and ions with different oxidation states and ionic radius [5]. These characteristics bring special attention to this material, once they allow the controlled modification of the STO structure at atomic level, targeting different characteristics and improving their properties. For instance, Fe can be introduced into the STO lattice [6], causing important modifications in its structure, and consequently in its properties [5,7], including the photocatalytic effectiveness promoting the degradation of common water contaminants, such as organic molecules, or water splitting.

In our research group, we have already carried out some studies about the synthesis of $SrTi_{1-y}Fe_yO_3$ (STFO) using microwave-assisted hydrothermal method [6]. Although STO has been synthesized by conventional hydrothermal method [4], to the best of our knowledge, STFO compounds synthesized by this method and the effect of Fe

* Corresponding author.
E-mail addresses: henriquepiau@yahoo.com.br, henrique.mourao@ict.ufvjm.edu.br (H.A.J.L. Mourão).

http://dx.doi.org/10.1016/j.mssp.2017.05.033
Received 7 October 2016; Received in revised form 28 April 2017; Accepted 31 May 2017
Available online 14 June 2017

addition on the photoactivity of $SrTiO_3$ were not reported in the literature. Therefore, this paper reports the synthesis of $SrTiO_3$ and $SrTi_{1-y}Fe_yO_3$ (STFO) by a conventional hydrothermal method, aiming to evaluate the effects of the substitution of Ti by Fe atoms, especially on the photoactivity towards the photodegradation of methylene blue (MB) dye under visible and UVC radiation. The properties of samples containing different amounts of Fe (2.5 mol%, 5 mol%, 10 mol%, 25 mol% and 45 mol%) were evaluated by X-ray Diffraction (XRD), X-ray absorption spectroscopy (XAS) and Mössbauer techniques.

2. Materials and methods

2.1. Hydrothermal syntheses of $SrTiO_3$ (STO) and $SrTi_{1-y}Fe_yO_3$ (STFO) samples

All the samples were synthesized by conventional hydrothermal method. For the synthesis of the STO sample, 1.07 g of $TiOSO_4{\cdot}yH_2SO_4{\cdot}yH_2O$ (99%, Sigma-Aldrich) was added to 50 mL of distilled water at around 50 °C under vigorous stirring. Then, 0.270 g of $SrCl_2{\cdot}2H_2O$ (99%, Sigma-Aldrich) was also added to this solution in order to obtain a 1:1 (Ti: Sr) molar proportion, corresponding to the stoichiometry of $SrTiO_3$. Finally, 50 mL of an aqueous KOH solution (KOH, 85%, Merck) of approximately 5.0 mol L^{-1} was slowly added to such solution under vigorous stirring.

For the synthesis of the STFO samples or $SrTi_{1-y}Fe_yO_3$, where y is the relative molar content of Fe with respect to Ti, $FeCl_3$ (97%, Sigma-Aldrich) reagent was used as the Fe source. An appropriate amount of $TiOSO_4{\cdot}yH_2SO_4{\cdot}yH_2O$ was added to 50 mL of distilled water at around 50 °C under vigorous stirring. Then, 0.270 g of $SrCl_2{\cdot}2H_2O$ and an appropriate amount of $FeCl_3$ were also added to this solution in order to obtain the proportions presented in Table 1. Finally, 50 mL of the KOH solution (5.0 mol L^{-1}) was added under heating and vigorous stirring. The $SrTi_{1-y}Fe_yO_3$ samples are referred to as STFO X%, where X is the percentage of Fe in the sample.

The precursor solutions were transferred into a Teflon vessel heated in a stainless steel autoclave at 140 °C for 60 min of hydrothermal treatment under mechanical stirring. After the hydrothermal treatment, all the synthesized materials were washed using distilled water and isopropyl alcohol. Then, the materials were oven-dried at 80 °C for 12 h to produce powder samples.

2.2. Characterization of the synthesized materials

In order to determine the crystalline phase of each sample, X-ray diffraction (XRD) patterns were collected in a Rigaku Rotaflex RU200B (Cu Kα radiation), at a scanning rate of 2° per min with 2θ ranging from 20° to 80°. The sample morphology was examined by field emission gun scanning electron microscopy (FEG-SEM) in a JEOL JSM 6701 F microscope. The semi quantitative atomic composition was evaluated by energy-dispersive X-ray (EDX) spectroscopy in an ultradry silicon drift detector (SDD) with a resolution of 132 eV coupled to a JEOL JSM 6510 microscope.

The diffuse reflectance data were obtained on a UV-2600 Shimadzu spectrophotometer, while the UV–Vis diffuse reflectance spectra (DRS) were transformed into the absorption spectra by using the Kubelka-Munk method [8]. The band gap energy values were calculated from the x-axis intercept of the tangent lines of each curve, as illustrated by the spectra presented in Fig. S2. The specific surface area (SSA) values of the STO, STFO 5% and STFO 40% samples were calculated via Brunauer-Emmett-Teller (BET) method using the N_2 adsorption data obtained in a Micromeritics ASAP-2020 equipment.

^{57}Fe Mössbauer transmission measurements were performed using a conventional constant-acceleration setup with Wissel and EG & G-Ortec electronics modules operating at room temperature with a ^{57}Co/Rh commercial source. Calibration has been performed with a standard α-Fe thin sample.

The variations in the electronic and local atomic structure around Ti atoms were studied by X-ray absorption spectroscopy (XAS). The XANES (X-ray absorption near-edge structure) part of the absorption spectra was measured at the titanium (Ti) K-edge using the D08B-XAS2 beam line at the Brazilian Synchrotron Light Laboratory (LNLS). The samples were deposited on polymeric membranes, and the XANES spectra were collected in transmission mode at room temperature with a Si (111) channel-cut monochromator. The XANES spectra were measured with an energy step of 0.3 eV around the near-edge region. In order to ensure better energy reproducibility for the collected spectra, the calibration of the monochromator was checked during data collection by means of a Ti metal foil target. All the data were normalized to the edge-step and aligned in energy. The XANES spectra were analyzed with the IFEFFIT package [9,10].

The photocatalytic performance of the as-synthesized materials was assessed by monitoring the degradation of the dye methylene blue (MB). Colloidal suspensions of the synthesized samples, at 200 mg L^{-1}, were prepared by dispersing 4.0 mg of the photocatalyst in 20.0 mL of MB aqueous solutions at 10.0 mg L^{-1}. Photodegradation tests were performed without mechanical stirring in a thermostated photoreactor at 20 °C under UV light irradiation by six UV-C lamps (TUV Philips, 15 W) with maximum emission at about 254 nm (Fig. S1), placed on the top of the reactor [11]. The decrease in the concentration of MB was monitored by UV absorption measurements at 665 nm in a Shimadzu UV-1601 PC spectrophotometer, after various light exposure times. So as to ensure that the adsorption equilibrium of MB molecules on the photocatalyst surface was reached, these suspensions were initially kept in the dark for 12 h. Using a similar procedure, the photoactivity of STO, STFO 5% and STFO 25% samples was also tested under visible radiation. The emission spectrum of the visible lamps is also presented in Fig. S1.

In order to check the stability of the samples, the STFO 10% sample was evaluated by reusing this material in three photocatalytic cycles under UVC light irradiation. After each reaction cycle, the sample was centrifuged and dispersed again in a new MB solution for another photocatalytic cycle.

Table 1
Amounts (in grams) of $TiOSO_4$ and $FeCl_3$ used for $SrTi_{1-y}Fe_yO_3$ (STFO) syntheses, y values and nominal amount of Fe (X mol% Fe) added during the synthesis.

m_{TiOSO4}/g	m_{FeCl3}/g	y	% Fe
1.040	0.0042	0.025	2.5
1.013	0.0085	0,05	5
0.959	0.0169	0.10	10
0.800	0.0426	0.25	25
0.639	0.0676	0.40	40

3. Results and discussion

3.1. Material characterization

The XRD patterns of the STO and some of STFO samples (5–40 mol %) presented in Fig. 1A show that all samples are fully crystallized, and the XRD patterns can be assigned to the $SrTiO_3$ cubic perovskite structure (JCPDS 35-0734, Fig. 1B). It is worth emphasizing that no peak associated with secondary phases containing elemental iron (Fe) can be observed in Fig. 1. However, STFO samples present diffraction peaks of lower intensity than the STO sample. This effect is clear for the STFO 40% sample and could be a result of an increase in the disorder caused by the substitution of Ti by Fe.

Fig. 2 shows representative STFO FEG-SEM images compared with those of STO, which show aggregates with a sphere-like morphology ranging from nanometric to micrometric sizes; however, it is also possible to observe the presence of some aggregates with faceted edges. Moreover, in accordance with our previous work, it can be noticed that

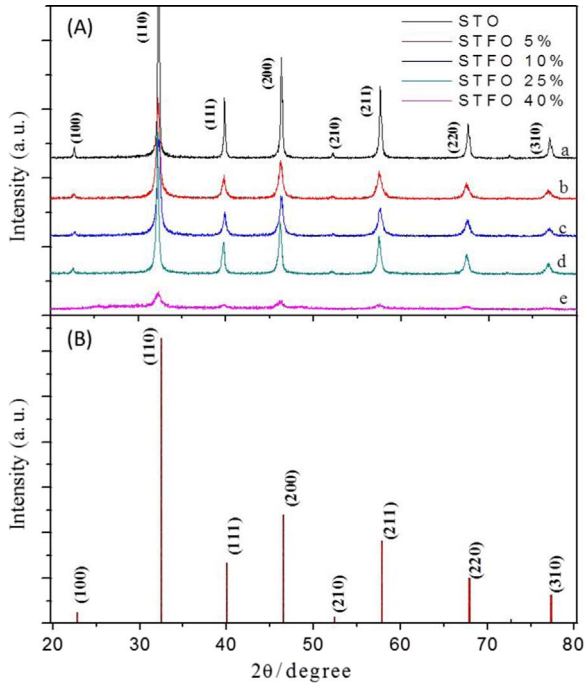

Fig. 1. (A) XRD patterns of STO (a) and some STFO samples with different molar proportions of Fe (b: 5%; c: 10%; d: 25%; e: 40%); (B) Standard diffraction peaks of the $SrTiO_3$ cubic perovskite structure (JCPDS 35-0734).

the spherical aggregates are composed of smaller nanoparticles with different shapes and sizes [4]. The STFO 10% nanoparticles do not show aggregates with faceted edges, and their surfaces are rougher compared to the STO nanoparticles. In both STFO 25% and STFO 40% samples, it is possible to observe a loss of shape and a greater surface roughness as the amount of Fe increases.

The semi-quantitative EDX analysis of the samples was performed to evaluate the presence of Sr, Ti and Fe in the as-synthesized samples. Fig. 3 presents a representative spectrum of the STFO 40% sample, whereas Table 2 shows the EDX results of the samples comparing the relative nominal proportions of Sr, Ti and Fe elements. From the last column, it is possible to observe that the amount of Fe was close to the nominal composition, especially for the STFO 10% sample. It is worth emphasizing that no significant amount of some elements, such as K, Cl and S (elements present in the reagents used in the synthesis), was observed in the EDX spectra. Although the EDX measurements cannot be used to prove that the replacement of Ti by Fe occurred in the STO lattice, it can be inferred that Fe was inserted, since no secondary phase containing Fe was observed in XRD patterns (Fig. 1).

In order to check the effect of Fe addition to the local and electronic structure, STO and SFTO samples were analyzed by XANES spectroscopy. As expected, the Ti K-edge XANES spectra (Fig. 4a) are similar to those found in previous reports concerning $SrTiO_3$ compound [7,12–15]. An analysis of expanded view from the pre-edge region evidences the presence of four typical pre-edge peaks, denoted as A, B, C1 and C2 (Fig. 4b) [14–17]. Several papers attributed the A peak to a pure quadrupole origin due to the 1 s(Ti)→3d(t_{2g})(Ti) transition, whereas the B peak was due to the 1 s(Ti) → 4p(Ti) transition, including some degrees of 1 s(Ti) → 3d(e_g)(Ti) quadrupole contribution, which is correlated to a five-coordinated titanium species (TiO_5) [14,15]. Additionally, the C_1 and C_2 peaks were assigned to a dipole excitation of 1 s electrons towards the t_{2g} and e_g orbitals of the neighboring TiO_6 octahedra [14,15,17]. It is interesting to note that a minor modification of both C_1 and C_2 peaks was observed, being it possibly related to a disturbance in the neighborhood of the TiO_6 octahedra caused by the addition of Fe atoms as second neighbors, also indicating that Fe was inserted into Ti sites. These effects are more pronounced in samples

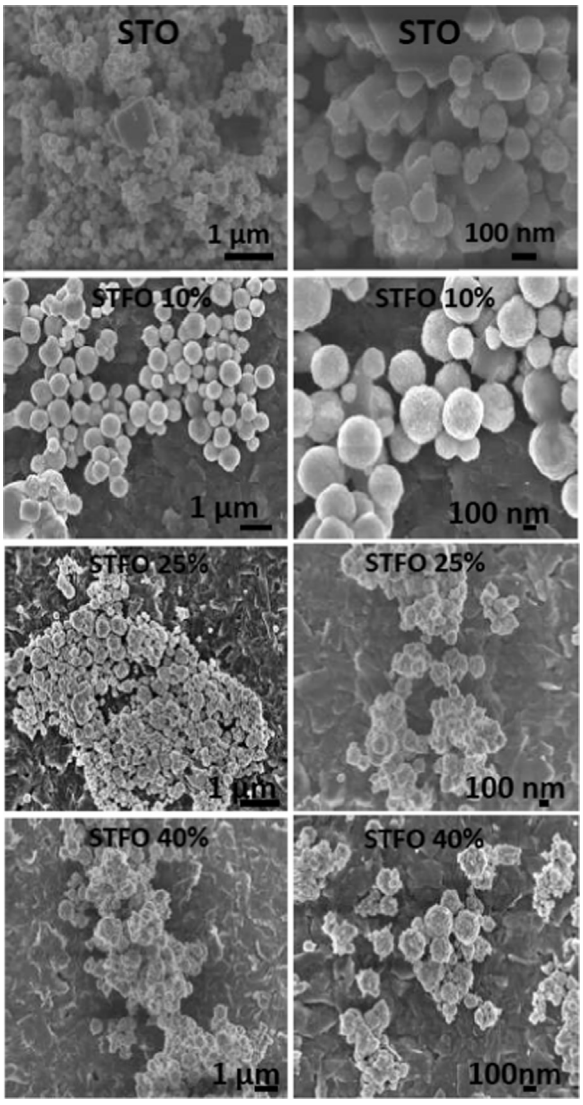

Fig. 2. Representative FEG-SEM images of STO and some STFO samples.

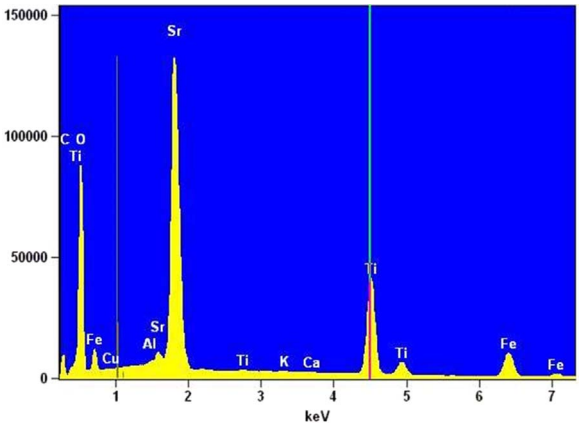

Fig. 3. EDX analysis of SFTO 40% sample identifying the peaks of Sr, Ti and Fe in the spectrum.

containing higher amounts of Fe. Furthermore, several studies indicated a relationship between the intensity of B peak and the local symmetry of Ti atoms, showing that an increase in such intensity is correlated to an increase in the local disorder of TiO_6 units [14–16]. In good agreement with previous work, the analysis of XANES results indicates that the Fe addition replacing Ti atoms lead to an increase of the local

Table 2
EDX data for relative mol contents of Sr, Ti, Fe and relative Ti proportion expressed as {%Ti/(%Ti+%Fe)} × 100% for some samples.

Sample/ Element	Sr (mol%)	Ti (mol%)	Fe (mol%)	{Ti/ (Ti+Fe)} × 100%
pure STO	51	49	0	100
STFO 10%	42	53	5	91
STFO 25%	44	45	11	80
STFO 40%	43	38	19	67

Note: 0 (zero) indicates a negligible value.

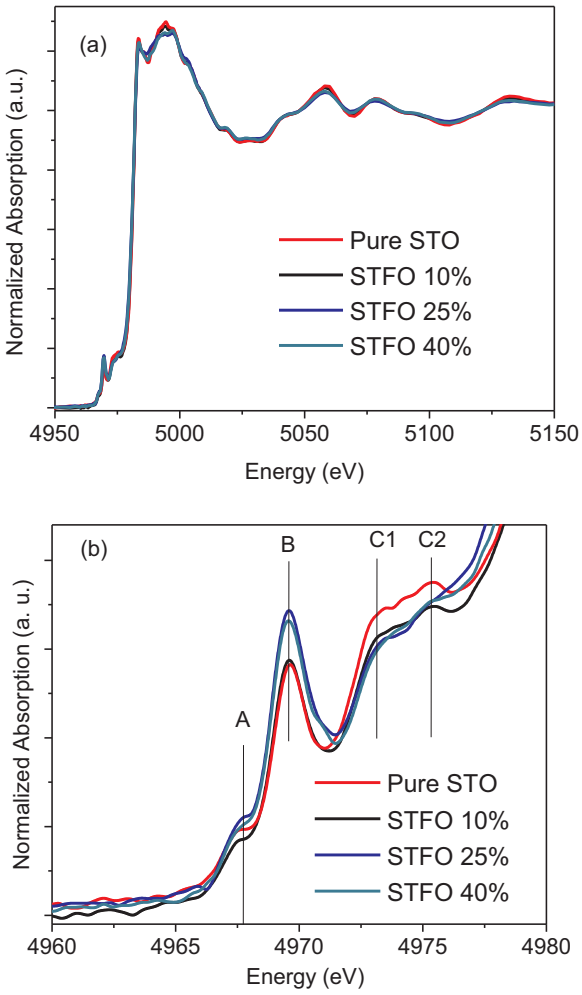

Fig. 4. (a) Normalized Ti K-edge XANES spectra and (b) expanded view of pre-edge feature of some synthesized samples.

disorder of TiO_6 units [17]. This corroborates with the observation of a decrease in the peak intensity in XRD patterns as the amount of Fe increases.

Mössbauer spectroscopy was used to determine the oxidation state of Fe ions, once this nuclear technique is very sensitive to the chemical environment around the probe nucleus, in our case ^{57}Fe [18,19]. About 2.2% of the natural isotopes of Fe are ^{57}Fe, consequently 2.2% of the inserted atoms are able to contribute to the Mössbauer signal. Since the isotopes are naturally distributed in a random way, their signals are representative of the different sites occupied by Fe atoms.

Fig. 5 shows the Mössbauer spectrum of the STFO 40% sample obtained at room temperature. The spectrum (with points) was fitted with two doublets (subspectra *a* and *b*), and the Mössbauer parameters are presented in Table 3. The isomer shifts and quadrupole splittings of these doublets are in the typical range for Fe^{3+} [20]. Their values are

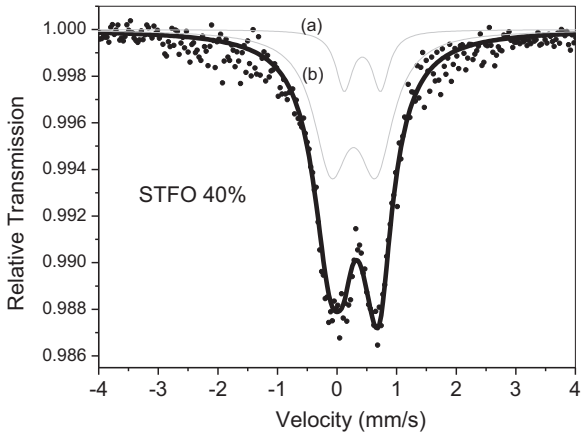

Fig. 5. Mössbauer spectrum (points) of the STFO 40% sample. The fitted curve (the thickest line) is the sum of two doublet contributions (subspectra *a* and *b*). The fitted parameters of each contribution are presented in Table 3.

Table 3
Fitted hyperfine parameters corresponding to two doublets (subspectra *a* and *b*) from Mössbauer spectrum of the STFO 40% sample.

Sample	Doublet	Isomer shift mm/s	Quadr. Split. mm/s	Area (%)
STFO 40%	(b) Fe^{3+} - V_O	0.18	0.75	90.3
	(a) Fe^{3+} - $V_{O(e)}$	0.32	0.61	9.7

very close to those expected when substituting Ti^{4+} by Fe^{3+} in its normal octahedral site, yet associated with an oxygen vacancy [18,19,21].

Different types of anion vacancies are commonly observed in $SrFeO_3$ [19,22], $BaTiO_3$ [23] and $SrTiO_3$ [21,24], and charge-compensating mechanisms lead to distinct couplings between the ion in the octahedral site and one or two electrons that can possibly occur at the vacancy. In a previous study of $SrTiO_3$ containing ^{57}Fe by Mössbauer spectroscopy, different Fe valences and anion vacancies could be observed [21] depending on the percentage of Fe and the sample thermal treatment. In good agreement with experimental results, Multani [18] presented a theoretical approach of such vacancies in Fe-doped $SrTiO_3$, showing that the quadrupole splitting is more affected by the presence or absence of electrons at the vacancies than is the isomer shift. Furthermore, details of the approach lead to a ± 0.1 mm/s uncertainty for the isomer shift and an uncertainty of approximately 30% for the quadrupole splitting [18].

The most intense Mössbauer doublet that was observed can then be attributed to Fe^{3+} in the octahedral sites associated with oxygen vacancies without unpaired electrons (Fe^{3+} - V_O), whereas the least intense doublet can be attributed to Fe^{3+} in the octahedral sites associated with oxygen vacancies with a single electron (Fe^{3+} - $V_{O(e)}$). These vacancies promote a significant axial distortion of the octahedral sites, explaining the Mössbauer results. The site distortion and coupling with the electron in some of the vacancies are also directly related to the results observed by the XRD and XANES experiments. From the Mössbauer measurements, it is also possible to disregard the presence of Fe^{2+} and Fe^{4+}, once the former is expected to result in an isomer shift around 1 mm/s (at least larger than 0.7 mm/s) and the latter is expected to present null or small negative isomer shifts. None of these values were detected in our sample. Moreover, elemental Fe or atomically dispersed Fe were not detected, since their presence in a significant amount would result in characteristic sextets or singlets signals in the Mössbauer spectrum.

Only the sample with the highest Fe content (40%) was characterized by Mössbauer spectroscopy for a better sensitivity. However, it is expected that the other samples (SFTO or STFO) present the same

Table 4
Band gap values of the synthesized samples: pure STO, STFO 5%, STFO 10%, STFO 25% and STFO 40%.

Samples	*Band gap (eV)*
STO	3.1
STFO 5%	3.0
STFO 10%	2.8
STFO 25%	2.3
STFO 40%	2.4

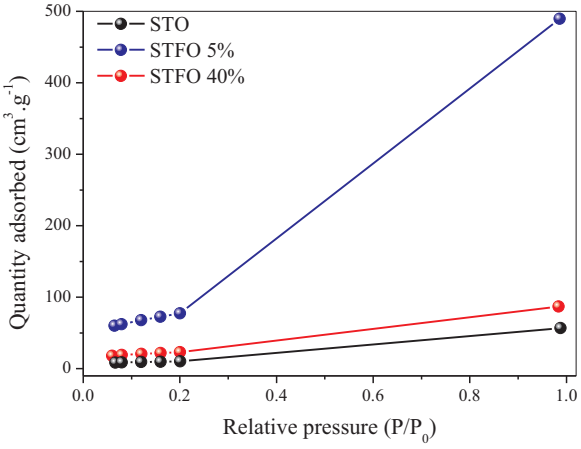

Fig. 6. N_2 adsorption isotherms obtained for the samples STO, STFO 5% and STFO 40%.

characteristics with respect to the valence and doped site.

The optical properties of the synthesized samples were studied by UV–Vis diffuse reflectance. Fig. S2 illustrates the plot of the absorption spectra used to obtain the band gap values presented in Table 4. The calculated band gap value of the STO was 3.1 eV, which was higher than the ones of the STFO samples. Additionally, the samples with the highest amounts of Fe (25 mol% and 40 mol%) showed the lowest values of band gap (2.3 and 2.4 eV, respectively). Thus, the values of band gap of the STFO suggest that these samples are photoactived by UV and visible radiation. Fig. 6 and Table 5 show, respectively, the N_2 adsorption isotherms and the values of the textural properties for some samples. As can be seen, the addition of Fe affected also the textural properties of the synthesized materials, causing the STFO samples to present a higher surface area (STFO 5% and STFO 40% of 281 m^2/g and 84 m^2/g, respectively) than the STO sample (36 m^2/g). The mesopore size (Dpore) is a useful feature for percolation of MB molecules to be degraded into the structure. Also, the STFO 5% exhibited mesoporous volume approximately 7 times higher than the pure STO sample, which provides a more efficient transport pathway to the surface active sites.

3.2. Photocatalytic activity of synthesized samples

As discussed before, the introduction of Fe^{3+} into Ti^{4+} sites of the $SrTiO_3$ lattice caused several changes in its structural, morphologic, textural and optical properties. The photodegradation of MB dye was used to evaluate the effect of these changes on the photoactivity of these materials and also to find the optimal proportion of Fe for the photoactivity. Fig. 7 shows the results of the photoactivity measurements under UVC irradiation for all the synthesized samples. In the Fig. 7a can be observed the MB dye spectra as function of exposure time to UVC radiation catalyzed by the STFO 5% sample. From the curves presented in Fig. 7b, it can be observed that the reaction presents a first-order characteristic [25,26]. Using the same procedure employed in our previous studies [25,26], the photodegradation curves were linearized by the pseudo-first-order model, as presented in Fig. 7c. The reaction constants were calculated, and the obtained results are presented in Table 6.

Table 5
Textural properties of some synthesized samples.

Sample	[a]SSA ($m^2\,g^{-1}$)	[b]D_{pore} (nm)	[c]V_{pore} ($cm^3\,g^{-1}$)
Pure STO	36	10	0.10
STFO 5%	281	11	0.76
STFO 40%	84	6	0.14

[a] SSA – BET specific surface area.
[b] D_{pore} – pore size.
[c] V_{pore} –pore volume.

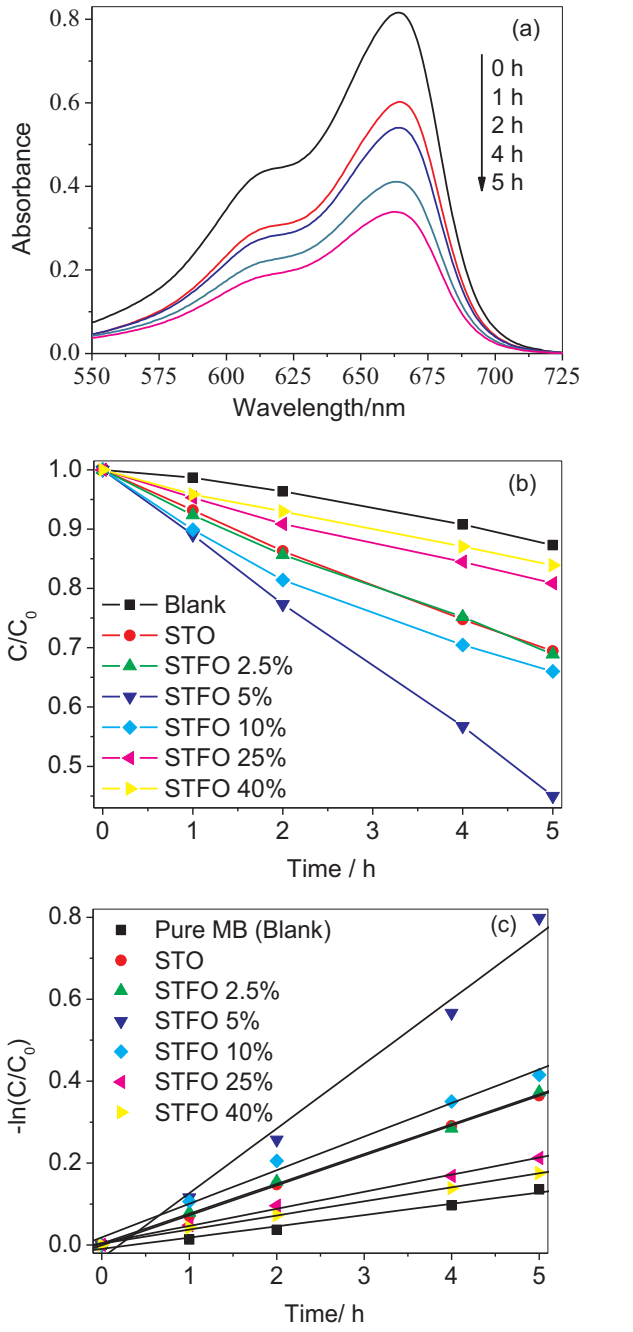

Fig. 7. (a) Time dependent absorption spectra of MB in presence of the sample STFO 5% during 5 h of photodegradation, (b) MB photodegradation curves catalyzed by as-synthesized samples and (c) the photodegradation reaction explained by first-order kinetic, under UVC light irradiation.

Table 6
First-order rate constants (*k*) for the MB photodegradation under UVC light irradiation.

Samples	*K* (h^{-1})	*R*
Blank	0.027	0.990
STO	0.073	0.999
STFO 2.5%	0.073	0.999
STFO 5%	**0.157**	0.994
STFO 10%	0.082	0.996
STFO 25%	0.044	0.998
STFO 40%	0.034	0.999

Note: *R* is the coefficient of determination for first-order kinetics.

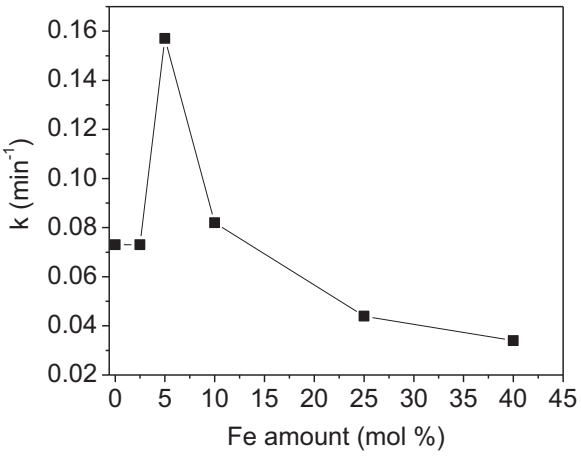

Fig. 8. Relationship between the values of MB photodegradation rate constant (k) and the amount Fe (in mol%), for photocatalytic test under UVC light irradiation.

According to Table 6, STO and STFO samples with different proportions of Fe were photoactive, since the curves are below pure MB curve (Blank) and their rate constants are larger than the MB rate constant (k = 0.027), which can be attributed to a direct photodegradation (without photocatalyst). The sample with the lowest amount of Fe (STFO 2.5%) showed photoactivity (k = 0.073) similar to the pure STO indicating that this amount of Fe is too low to increase the photoactivity of the STO compound. Besides, the rate constant of MB photodegradation in the presence of STFO 40% (k = 0.034) is almost equal to the MB direct photodegradation (Blank), indicating that higher amounts of Fe affect negatively the photoactivity compared to that of the STO sample. Additionally, only the samples with intermediate amounts of Fe show better performances than pure STO, i.e., the introduction of 5 mol% (k = 0.157) or 10 mol% (k = 0.082) of Fe improved the MB dye photodegradation when compared to that of the STO sample (k = 0.073). Fig. 8 shows this tendency and also that the 5 mol% is the optimal proportion of Fe substitution for MB photodegradation.

In semiconductor photocatalysis, the radiation must be able to photogenerate the charges, electron (e^-) and hole (h^+). However, e^- and h^+ are unstable with a short lifetime, and could undergo a recombination capable of preventing the photodegradation [27]. For such reasons, the recombination must be prevented. The UVC radiation used in the measurements presented in Fig. 7 and Table 6 has enough energy to photogenerate the charges, since the band gap of the samples are equal to 3.1 eV for STO and lower for all STFO samples. In this sense, the photogeneration of charges itself would not be able to explain the differences among the photoactivities of the synthesized samples. The difference among the textural properties could explain partly the variances among photoactivities since the STFO 5% sample is the best for both textural and photocatalytic properties. However, it could not explain the variances among all photoactivities, since the sample with 40 mol% of Fe shows surface area and pore volume higher than STO, even though its photoactivity is lower.

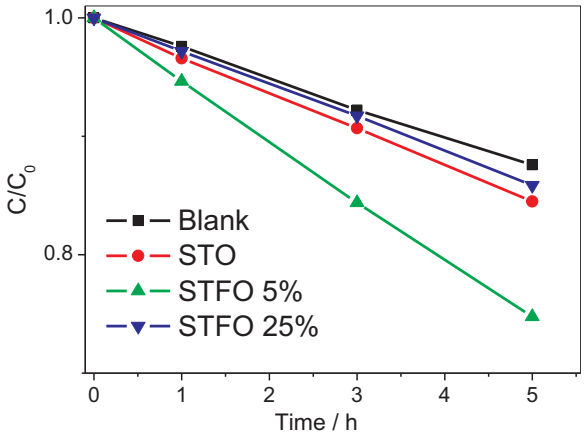

Fig. 9. MB photodegradation curves catalyzed by some as-synthesized samples (STO, STFO 5% and STFO 25%) under visible light irradiation.

To better understand the behavior of photoactivities presented by the synthesized samples, a complementary experiment was carried out by monitoring the photodegradation of the same molecule (MB dye) in the presence of some selected samples (STO, STFO 5% and STFO 25%) under visible light irradiation. The results are shown in Fig. 9 and Table 7. By the analysis of the band gap values presented in Table 4, both samples containing 5 mol% and 25 mol% of Fe are expected to be also photoactived by visible radiation. However, the values of rate constants of Blank (k = 0.026) are very close to those of STO (k = 0.034) and STFO 25% (k = 0.031) in Table 7, indicating no significant activity for these two samples under visible light. On the other hand, the rate constant of the STFO 5% sample is considerably larger (k = 0.059) than the previously cited samples. These results indicate that among the samples studied under visible irradiation only the STFO 5% sample showed significant activity. The photoactivity of the STFO 5% under visible light could be also explained by its good textural property.

In a previous study, it was proposed that the substitution of Ti^{4+} ions by Fe^{3+} can either increase the number of oxygen vacancies or defects, acting as electron traps, capturing the photo induced electrons, thus inhibiting the electron-hole recombination [28]. In another study, it was demonstrated that Fe-doped $SrTiO_3$ exhibited an absorption extending up to the visible region, which was attributed to the charge transfer of Ti to Fe [29]. Comparing these studies with our results, it is possible to point out some important considerations about the photoactivity of our synthesized samples. The improvement of the photoactivity of both 5 mol% and 10 mol% samples compared with that of STO could be related to three combined effects: the improved textural property; the electron-hole recombination decreasing; and the broadening of the absorption band of the photocatalyst, which is especially important for the photodegradation under visible irradiation. These effects occur due to the introduction of Fe into the STO structure. These positive characteristics were predominant for both 5 mol% and 10 mol % STFO samples and the best performance of sample STFO 5% was mainly attributed to its best textural properties. However, when the amount of Fe is high, disorder/defects could restrict the electron-hole

Table 7
First-order rate constants (*k*) for the MB photodegradation of some as-synthesized samples under visible light irradiation.

Samples	K (h^{-1})	R
Blank	0.026	0.999
STO	0.034	0.999
STFO 5%	0.059	0.999
STFO 25%	0.031	0.999

Note: *R* is the coefficient of determination for first-order kinetics.

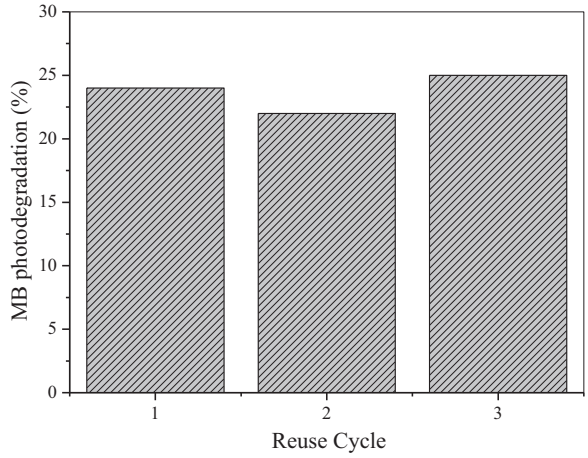

Fig. 10. Cyclic stability of the STFO 10% sample for MB removal.

photogeneration, which consequently proves to be negative for the photoactivity. In this study, this feature was related to the disorder caused by the introduction of 25 mol% and 40 mol% of Fe into the STO lattice, as showed by XRD, XANES and Mössbauer results.

Finally, the stability of the synthesized samples was evaluated by reusing the STFO 10% sample in three photocatalytic cycles under UVC irradiation. As presented in Fig. 10, the STFO 10% sample showed no significant deactivation even after three successive re-uses for the MB dye photodegradation. This is an important characteristic, since the stability of the photocatalyst under a photoreaction is a critical factor when considering its practical application.

4. Conclusions

This study presented a hydrothermal synthesis of $SrTiO_3$ (STO) and $SrTi_{1-y}Fe_yO_3$ (STFO) with different molar proportions of Fe, and the evaluation of their photoactivities under visible and UVC irradiation. The introduction of Fe^{3+} into Ti^{4+} sites changed the structural, optical, morphological, textural and photocatalytic properties of the STO compound. It was observed that STFO 5% and STFO 10% exhibited the better photocatalytic performance on MB dye photodegradation under UVC irradiation, probably due to an improvement in the textural properties and a decrease in the electron-hole recombination. Also, the addition of Fe caused a decrease in band gap values, which caused a displacement in absorption band to visible region. It was also observed that high amounts of Fe caused great changes in the morphology and crystal order structure, especially an increase in the local distortion around TiO_6 units, causing a negative effect on the photoactivity. Hence, our results show that the addition of Fe to STO lattice enhances its photoactivity for intermediate amounts of Fe and that 5 mol% is the optimal proportion for MB photodegradation. This good performance of STFO 5% was mainly due to its best textural properties.

Acknowledgements

The authors would like to acknowledge CNPq (503272/2011-6 and 454438/2014-1) and FAPESP (2012/11246-8, 2013/17639-4 and 2013/13888-0) for the financial support provided for this research, as well as the LNLS (Campinas, SP, Brazil) laboratories for XAS analyses (XAFS1-14284 and XAFS2-12470). We also would like to thank Professor José Domingos Fabris, member of a research group at UFVJM (Materials Science and Technology Group), for the Mössbauer analysis.

Appendix A. Supplementary material

Supplementary data associated with this article can be found in the online version at http://dx.doi.org/10.1016/j.mssp.2017.05.033.

References

[1] W. Dong, X. Li, J. Yu, W. Guo, B. Li, L. Tan, C. Li, J. Shi, G. Wang, Mater. Lett. 67 (2012) 131–134.
[2] Y. Hu, O.K. Tan, W. Cao, W. Zhu, Ceram. Int. 30 (2004) 1819–1822.
[3] S. Ahuja, R.N. Kutty, J. Photochem. Photobiol. A 97 (1996) 99–107.
[4] H.A.J.L. Mourão, O.F. Lopes, C. Ribeiro, V.R. Mastelaro, Mater. Sci. Semicond. Process. 30 (2015) 651–657.
[5] X. Zhou, J. Shi, C. Li, J. Phys. Chem. C 115 (2011) 8305–8311.
[6] L.F. da Silva, W. Avansi Jr, M.L. Moreira, J. Andrés, E. Longo, V.R. Mastelaro, Cryst. Eng. Comm. 14 (2012) 4068–4073.
[7] L.F. da Silva, W. Avansi Jr., J. Andres, C. Ribeiro, M.L. Moreira, E. Longo, V.R. Mastelaro, Phys. Chem. Chem. Phys. 15 (2013) 12386–12393.
[8] K. SUZUKI, K. KIJIMA, Jpn. J. Appl. Phys. 44 (2005) 2081–2082.
[9] M. Newville, J. Synchrotron Rad. 8 (2001) 322–324.
[10] M. Newville, J. Synchrotron Rad. 8 (2001) 96–100.
[11] O.F. Lopes, K.T.G. Carvalho, G.K. Macedo, V.R. de Mendonça, W. Avansi, C. Ribeiro, New J. Chem. 39 (2015) 6231–6237.
[12] M.ário L. Moreira, Valéria M. Longo, Waldir Avansi Jr., Mateus M. Ferrer, Juan Andrés, Valmor R. Mastelaro, José A. Varela, Élson Longo, J. Phys. Chem. C 116 (2012) 24792–24808.
[13] Luís F. da Silva, Waldir Avansi, M.ário L. Moreira, Alexandre Mesquita, Lauro J.Q. Maia, Juan Andrés, Elson Longo, Valmor R. Mastelaro, J. Nanomater. 2012 (2012) 6Article ID 890397.
[14] F. Farges, G.E. Brown, J.J. Rehr, Phys. Rev. B 56 (1997) 1809–1819.
[15] I. Levin, V. Krayzman, J.C. Woicik, A. Tkach, P.M. Vilarinho, Appl. Phys. Lett. 96 (2010) (052904-1-052904-3).
[16] H.A.J.L. Mourão, W. Avansi, J.E. Oliveira, E.S. Firmiano, C. Ribeiro, Sci. Adv. Mater. 5 (2013) 71–85.
[17] L.F. da Silva, J.-C. M'Peko, J. Andrés, A. Beltrán, L. Gracia, M.I.B. Bernardi, A. Mesquita, E. Antonelli, M.L. Moreira, V.R. Mastelaro, J. Phys. Chem. C. 118 (2014) 4930–4940.
[18] M. Multani, Mat. Res. Bull. 19 (1984) 25–34.
[19] P.K. Gallagher, J.B. MacChesney, D.N.E. Buchanan, J. Chem. Phys. 41 (1964) 2429–2434.
[20] N.N. Greenwood, T.C. Gibb, Mössbauer Spectroscopy, Chapman and Hall, London, 1971.
[21] V.G. Bhide, H.C. Bhasin, Phys. Rev. 172 (1968) 290–294.
[22] P.K. Gallagher, J.B. MacChesney, D.N.E. Buchanan, J. Chem. Phys. 45 (1966) 2466–2471.
[23] E. Mashkina, C. McCammon, F. Seifert, J. Solid State Chem. 177 (2004) 262–267.
[24] K.A. Müller, J. Phys. 42 (1981) 551–557.
[25] A.R. Malagutti, H.A.J.L. Mourão, J.R. Garbin, C. Ribeiro, Appl. Catal. B: Environ. 90 (2009) 205–212.
[26] H.A.J.L. Mourão, A.R. Malagutti, C. Ribeiro, Appl. Catal. A 383 (2010) 284–292.
[27] Henrique A.J.L. Mourão, Vagner R. de Mendonça, Andréa R. Malagutti, Caue Ribeiro, Quim. Nova 32 (2009) 2181–2190.
[28] M. Ghaffari, T. Liu, H. Huang, O.K. Tan, M. Shannon, Mater. Chem. Phys. 136 (2012) 347–357.
[29] Tai-Hua Xie, Xiaoyan Sun, Jun Lin, J. Phys. Chem. C 112 (2008) 9753–9759.